Research Square

Preprints are preliminary reports that have not undergone peer review.
They should not be considered conclusive, used to inform clinical practice,
or referenced by the media as validated information.

B7-H3, a marker related to angiogenesis in hepatocellular carcinoma, promotes contrast-enhanced ultrasound

haiying tian

tianhaiying@stu.gmc.edu.cn

Guizhou Provincial People's Hospital

ning ma

Guizhou Provincial People's Hospital

yuling chen

Guizhou Provincial People's Hospital

bei zhang

Affiliated Hospital of Guizhou Medical University

Article

Keywords: Hepatocellular carcinoma, B7-H3, NF-κB signaling pathway, Contrast-enhanced ultrasound

Posted Date: March 18th, 2026

DOI: https://doi.org/10.21203/rs.3.rs-8756128/v1

License: This work is licensed under a Creative Commons Attribution 4.0 International License.
Read Full License

Additional Declarations: No competing interests reported.

Abstract

B7-H3, a member of the B7 family of molecules, is a type I transmembrane glycoprotein that plays a critical role in the development and progression of various cancers. Our study demonstrates that B7-H3 functions as an oncogenic driver in hepatocellular carcinoma (HCC). Specifically, B7-H3 promotes tumor proliferation, migration, invasion, and angiogenesis in HCC. These effects were reversed upon inhibition of B7-H3. We further investigated the underlying mechanism and found that B7-H3 exerts its tumor-promoting functions by activating the NF-κB signaling pathway, thereby promoting the progression of HCC and the level of contrast-enhanced ultrasound. These findings provide a novel theoretical basis for understanding the pathogenesis of hepatocellular carcinoma.

Introduction

Hepatocellular carcinoma (HCC) is a prevalent malignancy of the digestive system, posing a severe threat to global human health due to its high incidence and mortality rates, which impose a substantial burden on society and families [1,2]. According to the 2022 global cancer burden data from the International Agency for Research on Cancer (IARC) of the World Health Organization [3,4], HCC accounted for approximately 866,000 new cases and 759,000 deaths worldwide, ranking as the sixth most common cancer and the third leading cause of cancer-related mortality. China, as a high-incidence region for HCC, reports the fourth highest incidence and second highest mortality among all cancers domestically, with an estimated 367,000 new cases and 316,000 deaths in 2022. Despite advancements in early diagnostic techniques, over 60% of patients are diagnosed with vascular invasion or distant metastasis, resulting in a five-year survival rate of less than 20% [5]. Thus, there is an urgent need to investigate the molecular mechanisms underlying HCC invasion and metastasis and to develop novel intervention strategies.

Current treatment modalities for HCC include surgical resection, liver transplantation, local ablation, transarterial chemoembolization (TACE), radiotherapy, chemotherapy, targeted therapy, and immunotherapy [6,7]. Surgical resection and liver transplantation remain the cornerstone curative approaches for early-stage patients. However, most patients are diagnosed at advanced stages and miss the window for surgical intervention. Moreover, postoperative recurrence rates remain high, limiting overall therapeutic efficacy. Local ablation and TACE are applicable to certain non-operable patients but have inherent limitations. Radiotherapy and chemotherapy offer limited efficacy and are associated with significant adverse effects. Although emerging targeted and immunotherapies have brought new hope [8], challenges such as drug resistance and low response rates persist. Therefore, identifying new therapeutic targets and strategies is crucial for improving outcomes and prognosis in HCC.

Recent studies have demonstrated that the B7 family of molecules plays a critical role in tumor immune evasion and the formation of the tumor microenvironment. Tumor cells can achieve immune escape by aberrantly expressing certain B7 family members [9]. Among them, B7-H3, which is highly expressed in HCC, is involved in the progression of various cancers. It not only inhibits the activity of T cells and NK

cells to facilitate immune evasion but also activates intracellular signaling pathways, thereby promoting HCC cell proliferation, invasion, migration, and tumor angiogenesis, all of which contribute to tumor growth and metastasis [10]. Furthermore, the NF-κB signaling pathway is frequently dysregulated in HCC and is closely associated with tumor initiation, progression, metastasis, and therapy resistance [11,12].

In this study, we first collected clinical samples to clarify the association between B7-H3 expression and clinicopathological parameters in HCC patients. Subsequently, we performed in vitro functional assays using siRNA-mediated knockdown and lentivirus-mediated overexpression to investigate the effects of B7-H3 on HCC cell proliferation, migration, and invasion. Xenograft tumor models in nude mice were established to examine the role of B7-H3 in tumor growth in vivo, with contrast-enhanced ultrasound employed to monitor tumor blood perfusion. Finally, through comprehensive in vitro and in vivo experiments, including rescue assays, we aimed to validate the biological functions of B7-H3 and explore its potential regulatory signaling pathways.

Materials and methods

Materials

HCC (HepG2, Huh7) cell line (Pricella); fetal bovine serum (FBS); penicillin–streptomycin, trypsin, DMEM (Gibco); PCNA, Ki67, VEGFA, CD31 antibodies (Proteintech); B7-H3(Abcam, Santa Cruz Biotechnology), p65, IκBα, IKKα/β (Abcam); mouse-derived secondary antibody, rabbit-derived secondary antibody (Abcam); TRIzol kit (Nitrogen); cDNA synthesis kit (Thermo Scientific); BCA working solution, RIPA lysis solution, PMSF, prestained Marker (Solarbio); CCK-8 kit ECL working solution, Matrigelgel, SDS-PAGE gel-making kit (Beyotime); B7-H3 overexpression lentivirus and negative control, B7-H3 small interfering RNA and negative control (Genechem); SonoVue (Bracco Suisse SA); NU/NU nude mice (Vital River) were used in this study.

Bioinformatics analysis

This study employed a multi-database integrative approach to characterize the expression profile of B7-H3. First, expression data matrices for this gene across various tumor types and corresponding normal tissues were precisely extracted from The Cancer Genome Atlas (TCGA) database, establishing a robust data foundation for pan-cancer differential expression analysis. Subsequently, the UALCAN online database was utilized to investigate differences in its protein expression levels across tissues, with a particular focus on determining its protein expression level in liver cancer tissues. Concurrently, the subcellular localization map of this protein was obtained from the Human Protein Atlas database, providing a spatial reference for subsequent functional studies.

Cell culture

In this study, Huh7 and HepG2 cells were cultured following standard protocols. For resuscitation, frozen cell vials were rapidly thawed in a 37–38°C water bath for 1–2 minutes, followed by surface disinfection,

centrifugation to remove the cryoprotectant, resuspension in complete medium, and seeding into culture vessels. When cells reached 80–90% confluence, they were passaged by removing the old medium, washing with PBS, detaching with trypsin, neutralizing the reaction with complete medium, centrifuging, and reseeding at a 1:2 – 1:3 split ratio. For cryopreservation, cells were harvested similarly, resuspended in pre-chilled freezing medium, subjected to controlled-rate cooling, and transferred to liquid nitrogen for long-term storage. Cell counting was performed by diluting the cell suspension, loading it onto a hemocytometer, counting cells in the four corner squares, and calculating the concentration using the standard formula.

Immuohistochemical stainin

For immunohistochemistry (IHC), 71 HCC tissue sections and 67 adjacent non-tumor tissue sections were processed. The procedure was conducted as follows: sections were first baked at 60°C for 3 hours, followed by deparaffinization in xylene, rehydration through a graded ethanol series, and rinsing with distilled water. Antigen retrieval was performed by incubating the sections in preheated retrieval buffer at 92–95°C under gentle boiling for 30 minutes, after which the slides were washed three times with PBS. Endogenous peroxidase activity was blocked by incubating with 3% hydrogen peroxide in the dark for 10 minutes. Nonspecific binding was blocked with 1% goat serum at room temperature for 30 minutes. The sections were then incubated overnight at 4°C (or for 1–2 hours at room temperature) with a primary antibody against B7-H3 diluted at 1:100. After PBS washes, a secondary antibody was applied and incubated at room temperature for 1 hour, followed by further rinsing. Subsequently, the slides were incubated with HRP-conjugated streptavidin, washed with PBS, and developed with DAB under microscopic monitoring. Counterstaining was performed with hematoxylin, and slides were rinsed with deionized water, dehydrated through a graded ethanol series, cleared in xylene, and mounted with neutral resin. Quantitative evaluation was performed using the H-Score system, which integrates both staining intensity and the percentage of positive cells.

Lentivirus infection

Cells were seeded in six-well plates at a density of 1×10^5 cells per well and cultured for 16–20 hours until reaching 20–30% confluence. For lentiviral transduction, a viral mixture was prepared by combining 5 μL of viral stock solution, 40 μL of GP reagent (enhanced transduction reagent), and complete medium to a final volume of 500 μL, achieving a multiplicity of infection (MOI) of 50. The old medium was aspirated, and cells were gently washed with PBS. Subsequently, the prepared mixture was added to each well, and the plate was rocked gently in a cross pattern to ensure even distribution. Cells were then cultured for 48–72 hours. Transduction efficiency was assessed by observing GFP fluorescence under a fluorescence microscope.

After 48 hours, total RNA was extracted and subjected to RT-qPCR to evaluate the efficiency of gene regulation. If the desired knockdown or overexpression efficiency was not achieved, puromycin selection

was initiated at 72 hours post-transduction. Once satisfactory regulatory efficiency and appropriate cell density were confirmed, subsequent functional assays were performed.

siRNA transfection

Cells in the logarithmic growth phase were seeded into six-well plates at a density of 3×10^5 cells per well and cultured at 37°C under 5% CO_2 for 16–24 hours until reaching 30–50% confluence. After labeling according to experimental groups, the medium was replaced with 1 mL of fresh complete medium per well. For transfection, siRNA and the Wibomix reagent were separately diluted in high-glucose DMEM in sterile microcentrifuge tubes. The diluted solutions were then combined, mixed gently, and incubated at room temperature for 10–15 minutes to allow complex formation. The resulting transfection complexes were added dropwise to the corresponding wells, and the plates were gently rocked in a cross pattern to ensure even distribution. Cells were subsequently cultured for 4–6 hours, with close monitoring of their morphological status. Knockdown efficiency was assessed 24–72 hours post-transfection. Once satisfactory knockdown (typically confirmed at 48–72 hours) and appropriate cell conditions were achieved, subsequent functional experiments were conducted.

RT-qPCR

Total RNA was extracted using the TRIzol reagent kit. cDNA was synthesized from the extracted RNA with a commercial cDNA synthesis kit. Subsequently, quantitative real-time PCR (qRT-PCR) was performed using specific primers to amplify the target sequences, with β-actin serving as the internal reference gene. The relative expression levels of RNA were calculated using the $2 - \Delta\Delta Ct$ method.

Western blot

HCC tissue samples were maintained on ice and lysed with RIPA lysis buffer for 30 minutes, followed by sonication. The lysates were then centrifuged at 12,000 r/min for 15 minutes at 4°C, and the supernatant was collected. The total protein concentration was determined using the bicinchoninic acid (BCA) assay. Equal amounts of protein from each group were separated by SDS-PAGE and subsequently transferred onto a membrane. After washing, the membrane was blocked for 2 hours. Following blocking, the membrane was incubated overnight at 4°C with a diluted primary antibody. After washing again, a secondary antibody was applied and incubated at room temperature for 2 hours, followed by further washing. Finally, protein bands were visualized using an enhanced chemiluminescence (ECL) kit, and the expression levels of the target proteins were analyzed accordingly.

Cell proliferation assay

Cell proliferation was assessed using the Cell Counting Kit-8 (CCK-8) assay. Briefly, HCC cells were seeded into 96-well plates at a density of 4×10^3 cells per well in 100 μL of culture medium, with four

replicate wells per experimental group. At the indicated time points (6, 24, 48, and 72 hours), 10 μL of CCK-8 reagent was added to each well, followed by incubation at 37°C for 1.5 hours. The absorbance of each well was then measured at a wavelength of 450 nm. The optical density (OD) values were recorded at each time point for subsequent analysis.

Colony formation assay

The colony formation assay was performed as follows: HCC cells were seeded into 6-well plates at a density of 1 × 10^3 cells per well and cultured in medium supplemented with 10% fetal bovine serum (FBS) for 14 days. Subsequently, the cells were washed with PBS, fixed with 4% paraformaldehyde for 20 minutes, and stained with 0.1% crystal violet for another 20 minutes. Colony formation was then observed and quantified under a light microscope.

Wound healing assay

A wound-healing assay was performed to evaluate cell migration. HCC cells were seeded into 12-well plates and cultured in a standard incubator until reaching 100% confluence. A straight scratch was created in each well using a sterile 200 μL pipette tip. The original medium was then discarded, and the cells were gently washed with PBS. Subsequently, 1 mL of serum-free DMEM medium was added to each well, and the plates were returned to the incubator for continued culture. The migration of cells into the wound area was monitored and photographed under a microscope at 0, 24, 48, and 72 hours post-scratch.

Transwell assays

For cell migration and invasion assays, HCC cells were first digested and resuspended in serum-free DMEM medium. The cell suspension was then seeded into the upper chamber of a Transwell insert at a density of 5×10^4 cells per well. For the invasion assay specifically, Matrigel was thawed, diluted 1:10 with DMEM, and 50 μL of the diluted Matrigel was applied to the upper chamber, followed by incubation at 37°C for 2 hours to form a gel layer. The chambers were subsequently placed in a regular incubator and cultured for 48 hours (migration assay) or 72 hours (invasion assay). After incubation, the medium in the upper chamber was removed. Cells were washed with PBS, fixed with 4% formaldehyde for 20 minutes, and stained with 0.1% crystal violet for another 20 minutes. Following another PBS wash, non-migrated or non-invaded cells on the upper surface of the membrane were gently removed using a cotton swab. The number of migrated or invaded cells on the lower surface was counted in five randomly selected fields under an inverted microscope.

Subcutaneous tumor model in nude mice

A subcutaneous xenograft tumor model was established in nude mice. Huh7 cells stably overexpressing B7-H3 or corresponding control cells (5×10^6 cells per mouse) were suspended in PBS and subcutaneously injected into the dorsal flank of female NU/NU nude mice (18-22g, 4 weeks old, n = 7 per group). Tumor growth was monitored every three days by measuring tumor dimensions with a caliper,

and the volume was calculated using the formula: Volume = (length × width²) / 2. When the tumors reached an appropriate size (e.g., 5–10 mm in diameter), subsequent experiments such as contrast-enhanced ultrasound imaging or tissue harvesting were performed according to the experimental design. Mice were euthanized by CO_2 inhalation at a flow rate of 20% chamber volume per minute, followed by 5 minutes of exposure to 100% CO_2. Death was confirmed by absence of respiration and corneal reflex. All procedures were approved by the Institutional Animal Care and Use Committee.

Contrast-enhanced ultrasound

When the xenograft tumors reached an appropriate size (generally with a diameter of 5–8 mm), the tail vein of the nude mouse was selected as the injection site. The skin around the tail vein was disinfected with iodophor. An appropriate volume of diluted contrast agent was drawn using a 1 mL syringe. The needle was inserted slowly and parallel to the tail vein. After confirming that the needle was correctly positioned within the vessel, the contrast agent was rapidly injected at a typical dose of 0.1–0.2 mL/kg. Simultaneously with the injection, the contrast-enhanced imaging mode of the ultrasound diagnostic system was activated to initiate real-time observation of contrast perfusion within the transplanted tumor. Observations included the time to initial contrast perfusion, the sequence of perfusion, enhancement intensity, uniformity of enhancement, and washout time.

Statistical analysis

Experimental results are expressed as the mean ± standard deviation (SD). Statistical analyses were performed using GraphPad Prism (version 10.0.0) or R language (version 4.2.1). Comparisons between two groups were conducted using a two-tailed Student's t-test. For comparisons among multiple groups, one-way analysis of variance (ANOVA) was employed. Categorical data were assessed using the Chi-square test. All experiments were independently repeated at least three times to ensure data reliability. A P-value of less than 0.05 ($P < 0.05$) was considered statistically significant.

Results

From Bioinformatic Analysis to Tissue Expression: The Clinical Significance of B7-H3 in HCC

First, gene expression data for B7-H3 across 33 cancer types and their corresponding adjacent normal tissues were retrieved from TCGA. Analysis revealed that B7-H3 expression was significantly elevated in nearly all cancer types compared to normal tissues (Fig. 1A). To characterize the protein expression profile of B7-H3 in liver cancer, the subcellular localization of B7-H3 was examined using the Human Protein Atlas (HPA) database. Database queries indicated that B7-H3 is primarily localized to the cell membrane (Fig. 1B). Further analysis of the tumor tissue protein expression data within HPA showed that B7-H3 protein exhibited moderate to strong nuclear staining intensity in most tumor samples (Fig. 1C). Subsequent investigation using the UALCAN online database demonstrated a significant

upregulation of B7-H3 protein expression in HCC tissues compared to normal liver samples. Moreover, high B7-H3 expression was associated with more advanced clinical stages in HCC patients (Fig. 1D-F).

To validate the findings from the database analyses, this study collected 71 HCC tumor tissue samples and 67 paired adjacent non-tumor tissue samples from our hospital, which were then processed into pathological sections (Table 1). Immunohistochemistry (IHC) was performed to verify the differential expression of B7-H3 between tumor and adjacent tissues (Fig. 1G). The experimental results confirmed the predominant membranous localization of B7-H3 protein. Consistent with the bioinformatics predictions, B7-H3 protein expression was markedly higher in HCC tissues compared to adjacent non-tumor tissues.

Table 1
The correlation between B7-H3 expression levels and clinicopathological characteristics in HCC patients

Characteristics	n	B7-H3 expression		*P*
		Low (n = 32)	High (n = 39)	
Gender				0.311
Female	14	8	6	
Male	57	24	33	
Age (year)				0.113
≤50	18	11	7	
>50	53	21	32	
ACJJ clinical stage				0.017
I	40	23	17	
II-III	31	9	22	
Histological Grade				0.169
I- II	38	20	18	
III	33	12	21	
Tumor scale (cm)				0.086
≤5	39	14	25	
>5	32	18	14	
HBsAg				0.099
Positive	59	24	35	
Negative	12	8	4	
AFP (ug/L)				0.136
≤200	42	22	20	
>200	29	10	19	
Tumor thrombus				0.444
With	21	8	13	
Without	50	24	26	
Tumor encapsulation				0.722
With	45	21	24	
Without	26	11	15	
Microvascular invasion				0.007
With	37	11	26	
Without	34	21	13	

Establishment of B7-H3-overexpression and B7-H3-silenced cell line models in HCC cells

To further investigate the biological functions of B7-H3 in HCC, we established stable B7-H3-overexpressing human HCC cell lines (Huh7 and HepG2) using a lentiviral vector system. Transfection efficiency was confirmed by RT-qPCR and western blot analysis, which demonstrated significant increases in both B7-H3 mRNA and protein levels in the transduced cells (Fig. 2A,B). To specifically silence B7-H3 expression, two distinct siRNAs (si1-B7-H3 and si2-B7-H3) targeting non-overlapping regions of the B7-H3 mRNA were designed and transfected into Huh7 and HepG2 cells. Both siRNAs effectively downregulated B7-H3 expression at the mRNA and protein levels, confirming successful gene knockdown while minimizing potential off-target effects (Fig. 2C,D).

Subsequently, the impact of B7-H3 on HCC cell proliferation was assessed. Using the Cell Counting Kit-8 (CCK-8) assay and colony formation experiments, we found that B7-H3 overexpression significantly enhanced the proliferative capacity of both Huh7 and HepG2 cells. Conversely, knockdown of B7-H3 expression markedly inhibited the growth and proliferation of these HCC cell lines, as consistently demonstrated by both the CCK-8 and colony formation assays (Fig. 2E,F).

B7-H3 promotes HCC cell migration and invasion

A wound healing assay was performed to evaluate cell migration. The results demonstrated that overexpression of B7-H3 significantly enhanced the migratory capacity of both Huh7 and HepG2 hepatocellular carcinoma cells. Conversely, knockdown of B7-H3 markedly suppressed their migratory activity (Fig. 3A). To further investigate the impact of B7-H3 on the motile behavior of HCC cells, Transwell migration and invasion assays were conducted. The findings revealed that B7-H3 overexpression notably promoted the migration and invasion capabilities of Huh7 and HepG2 cells, indicating its role in driving HCC cell motility and invasiveness. In contrast, knockdown of B7-H3 led to a significant inhibition of both migration and invasion in these cell lines, as evidenced by the Transwell assays (Fig. 3B).

Establishment of a xenograft tumor model in nude mice and detection of related proteins

Results from the subcutaneous xenograft model in nude mice demonstrated that tumors derived from B7-H3-overexpressing Huh7 cells exhibited increased volume and mass compared to the control group (Fig. 4A). The expression of the angiogenesis-related protein VEGFA was elevated upon B7-H3 overexpression and reduced upon B7-H3 knockdown, indicating that B7-H3 promotes angiogenesis in liver cancer cells (Fig. 4B). Western blot analysis revealed that elevated B7-H3 expression in HCC cells promoted the phosphorylation of NF-κB pathway proteins, including p65, IκBα, and IKKα/β, whereas B7-H3 inhibition yielded the opposite effect (Fig. 4C).

IHC staining further demonstrated a significant enhancement in VEGFA-positive signal intensity within the xenograft tumors of the B7-H3 overexpression group. In the tumor parenchyma, a large number of tumor cells displayed strong positive staining, with densely distributed positive cells. Concurrently, CD31 staining, indicated by a brown signal, was more pronounced in this group compared to controls (Fig. 4D). Collectively, these findings underscore the important role of B7-H3 in promoting tumor angiogenesis.

Histopathological examination via H&E staining of tumor tissues from the B7-H3 overexpression group revealed characteristic malignant features. Tumor cells were densely and disorderly packed, with enlarged, hyperchromatic, and irregular nuclei. Frequent mitotic figures were observed, suggesting highly active proliferation. IHC analysis showed widespread and intense nuclear staining for PCNA throughout the tumor masses in the B7-H3 overexpression group. Under high-power magnification, most nuclei, particularly in densely cellular areas and at the tumor periphery, exhibited strong brown-yellow staining, indicating a very high proportion of positive cells. Similarly, Ki-67 positive staining, manifested as brown nuclear signal, was extensively distributed across the tumor tissue (Fig. 4E).

Evaluation of the correlation between B7-H3 expression and CEUS features in HCC patients and in a nude mouse xenograft model

Based on clinically collected data from HCC patients, we assessed the correlation between B7-H3 expression and its clinical significance in HCC. The results indicated that the expression level of B7-H3 showed a certain correlation with the CEUS enhancement intensity in patients (Fig. 5A,B). Furthermore, we performed CEUS on xenograft tumors in nude mice. Compared with the control group, the B7-H3 overexpression group exhibited increased peak intensity, heightened sharpness (rate of perfusion), and a larger area under the curve (AUC, reflecting total perfusion volume), while the time to peak (TTP) was significantly shortened. These findings suggest that B7-H3 overexpression promotes tumor angiogenesis and enhances hemodynamic perfusion (Fig. 5C-E).

Disscussion

HCC remains a major global health threat with a pathogenesis that is highly complex and not yet fully understood [13, 14]. Analysis of cancer tissue protein expression data from the HPA reveals moderate to strong B7-H3 protein staining in the vast majority of tumor tissues, in contrast to absent or weak staining in normal tissues, resulting in significantly higher H-scores in tumors. Consistently, data from TCGA indicate elevated B7-H3 mRNA expression in HCC tissues. IHC performed on 71 HCC and 67 paired adjacent non-tumor tissue sections collected from our hospital further confirmed that B7-H3 is primarily localized to the cell membrane and its protein expression is significantly higher in HCC tissues compared to adjacent tissues. This series of findings clearly demonstrates the tumor-specific overexpression of B7-H3 in HCC, suggesting it is a significant molecular event in hepatocarcinogenesis and implies a crucial role for B7-H3 in HCC pathology. In line with studies in other cancers [15, 16–18], B7-H3 is overexpressed in multiple tumor types, indicating it may be a broadly significant tumor-associated molecule. Analysis of baseline clinical data from HCC patients showed that B7-H3

expression levels closely correlate with advanced clinical stage and the presence of MVI. This suggests that patients with high B7-H3 expression are more likely to present at a later disease stage and with MVI, both of which are critical negative prognostic factors in HCC. These clinical associations further indicate that B7-H3 drives HCC progression, potentially by promoting tumor cell invasion and metastasis, leading to disease deterioration.

Functional investigations using CCK-8 and colony formation assays demonstrated that B7-H3 overexpression significantly enhanced the proliferative capacity of Huh7 and HepG2 cells, whereas B7-H3 knockdown markedly inhibited it. Similarly, wound healing, Transwell migration, and invasion assays revealed that B7-H3 overexpression significantly increased the migratory and invasive abilities of these cells, while its knockdown produced the opposite effect. These results strongly indicate that B7-H3 plays a pivotal role in promoting HCC cell migration and invasion. During metastasis, cancer cells must breach the basement membrane, migrate into surrounding tissues, and intravasate into blood or lymphatic vessels [19, 20]. B7-H3 may facilitate this process by modulating the expression of cell adhesion molecules, thereby altering cell-cell and cell-extracellular matrix interactions.

Western blot analysis indicated that B7-H3 overexpression upregulated, while its knockdown downregulated, the expression of the angiogenesis-related protein VEGFA, suggesting B7-H3 promotes tumor angiogenesis. Angiogenesis is essential for tumor growth and metastasis, supplying nutrients and oxygen and creating a route for hematogenous dissemination [21, 22]. B7-H3 may accelerate this process by upregulating VEGFA, thereby stimulating endothelial cell proliferation, migration, and tube formation, and fostering a favorable microenvironment for HCC progression. Further mechanistic investigation via Western blot showed that B7-H3 overexpression promoted the phosphorylation of key NF-κB pathway proteins (p65, IκBα, and IKKα/β), while B7-H3 inhibition had the opposite effect. The NF-κB pathway is a critical signaling cascade regulating diverse cellular processes including proliferation, survival, and immune responses [23]. B7-H3 likely influences multiple malignant phenotypes of HCC cells, such as enhancing proliferation, migration, and invasion, by modulating NF-κB activity. The link between B7-H3 and the NF-κB pathway is well-documented in various cancers, where B7-H3 regulates tumor growth and invasion through pathways like PI3K/AKT/STAT3, JAK2/STAT3, or NF-κB [24]. For instance, in breast cancer, B7-H3 activates NF-κB to promote DNA topoisomerase IIα expression, affecting chemosensitivity [25]. In HCC, B7-H3 overexpression may activate NF-κB to upregulate anti-apoptotic proteins like Bcl-2 and Bcl-XL, inhibiting apoptosis [26].

In clinical practice and research, CEUS is an invaluable imaging technique for dynamically assessing tumor microvascular perfusion, and its role in characterizing tumor biology is increasingly recognized [27, 28]. Our analysis of CEUS enhancement patterns in HCC patients revealed an association between B7-H3 expression levels and imaging features: tumors with high B7-H3 expression exhibited stronger arterial phase enhancement compared to those with low expression, reflecting abnormally rich blood supply. From a molecular perspective, this hyper-enhancement likely stems from B7-H3-driven aberrant angiogenesis. CEUS of xenograft tumors provides a direct, efficient, and reliable non-invasive means to study this effect [29, 30]. Real-time observation and quantitative analysis of perfusion parameters (e.g.,

peak intensity, TTP, sharpness, and AUC) demonstrated that B7-H3 significantly influences tumor vascularization.

In conclusion, the upregulation of B7-H3 appears to be a key factor contributing to the malignant behavior of HCC, potentially mediated through the activation of the NF-κB signaling pathway to promote proliferation, invasion, migration, and angiogenesis. These findings enhance our understanding of HCC pathogenesis and may offer novel perspectives for preventing and treating HCC metastasis.

Ethics statement The study was approved by the Ethics Committee of Guizhou Provincial People's Hospital. All subjects gave written informed consent and the study was performed following the ethical guidelines of the Declaration of Helsinki. The animal study was reviewed and approved by the Research Ethics Committee of Guizhou Provincial People's Hospital. This study was carried out in accordance with the recommendations in the Guide for the Care and Use of Laboratory Animals of the National Institutes of Health.

Declarations

Conflict of interest:

No potential conflict of interest was reported by the authors.

Funding:

This work was supported by the National Natural Science Foundation of China (No. 82360354); Guizhou Provincial Science and Technology Department (qiankehejichu-ZK[2022]yiban257); Guizhou Science and Technology Department (qiankehejichu-ZK(2024)zhongdian045).

Author Contribution

H. Tian: Funding acquisition, Methodology, Resources, Software, Writing – original draft. N. Ma: Formal analysis, Methodology, Writing – review & editing. Y. Chen: Data curation, Investigation, Project administration, Writing – review & editing. B. Zhang: Methodology, Visualization, Writing – review & editing.

Data Availability

The datasets used and analysed during the current study available from the corresponding author on reasonable request.

References

1. Toh, M. R. et al. Global Epidemiology and Genetics of Hepatocellular Carcinoma. *Gastroenterology* **164** (5), 766–782 (2023).
2. Singal, A. G., Kanwal, F. & Llovet, J. M. Global trends in hepatocellular carcinoma epidemiology: implications for screening, prevention and therapy. *Nat. Rev. Clin. Oncol.* **20** (12), 864–884 (2023).
3. Bray, F. et al. Global cancer statistics 2022: GLOBOCAN estimates of incidence and mortality worldwide for 36 cancers in 185 countries. *CA Cancer J. Clin.* **74** (3), 229–263 (2024 May-Jun).
4. Bray, F. et al. Global cancer statistics 2022: GLOBOCAN estimates of incidence and mortality worldwide for 36 cancers in 185 countries. *CA Cancer J. Clin.* **74** (3), 229–263 (2024).
5. Erstad, D. J. & Tanabe, K. K. Prognostic and Therapeutic Implications of Microvascular Invasion in Hepatocellular Carcinoma. *Ann. Surg. Oncol.* **26** (5), 1474–1493 (2019).
6. Han, Z. et al. Sorafenib combined with TACE improves survival in patients with hepatocellular carcinoma with vascular invasion. *Biosci. Trends*. **18** (5), 457–464 (2024).
7. Brown, Z. J. et al. Management of Hepatocellular Carcinoma: A Review. *JAMA Surg.* **158** (4), 410–420 (2023).
8. Shen, K. Y., Zhu, Y., Xie, S. Z. & Qin, L. X. Immunosuppressive tumor microenvironment and immunotherapy of hepatocellular carcinoma: current status and prospectives. *J. Hematol. Oncol.* **17** (1), 25 (2024). Published 2024 Apr 29.
9. Upadhaya, S., Neftelinov, S. T., Hodge, J. & Campbell, J. Challenges and opportunities in the PD1/PDL1 inhibitor clinical trial landscape. *Nat. Rev. Drug Discov*. **21** (7), 482–483 (2022).
10. Zhou, Z. et al. Inhibition of the B7-H3 immune checkpoint limits hepatocellular carcinoma progression by enhancing T lymphocyte-mediated immune cytotoxicity in vitro and in vivo. *Clin. Transl Oncol.* **25** (4), 1067–1079 (2023).
11. Ji, Y. et al. ESRP1-mediated biogenesis of circPTPN12 inhibits hepatocellular carcinoma progression by PDLIM2/ NF-κB pathway. *Mol. Cancer*. **23** (1), 143 (2024).
12. Zhu, T. et al. COMMD3 Expression Affects Angiogenesis through the HIF1α/VEGF/NF-κB Signaling Pathway in Hepatocellular Carcinoma In Vitro and In Vivo. *Oxid. Med. Cell. Longev.* **2022**, 1655502 (2022).
13. Zheng, J. et al. Hepatocellular carcinoma: signaling pathways and therapeutic advances. *Signal. Transduct. Target. Ther.* **10** (1), 35 (2025).
14. Foglia, B., Turato, C. & Cannito, S. Hepatocellular Carcinoma: Latest Research in Pathogenesis, Detection and Treatment. *Int. J. Mol. Sci.* **24** (15), 12224 (2023). Published 2023 Jul 31.
15. Zhao, B. et al. Immune checkpoint of B7-H3 in cancer: from immunology to clinical immunotherapy. *J. Hematol. Oncol.* **15** (1), 153 (2022).
16. Guo, C. et al. B7-H3 as a Therapeutic Target in Advanced Prostate Cancer. *Eur. Urol.* **83** (3), 224–238 (2023).

17. Miyamoto, T. et al. B7-H3 Suppresses Antitumor Immunity via the CCL2-CCR2-M2 Macrophage Axis and Contributes to Ovarian Cancer Progression. *Cancer Immunol. Res.* **10** (1), 56–69 (2022).
18. Zhang, H., Zhu, M., Zhao, A., Shi, T. & Xi, Q. B7-H3 regulates anti-tumor immunity and promotes tumor development in colorectal cancer. *Biochim. Biophys. Acta Rev. Cancer*. **1879** (1), 189031 (2024).
19. Feng, R., Chen, Y., Liu, Y., Zhou, Q. & Zhang, W. The role of B7-H3 in tumors and its potential in clinical application. *Int. Immunopharmacol.* **101**, 108153 (2021). Pt B).
20. Wu, S., Hu, C., Hui, K. & Jiang, X. Non-immune functions of B7-H3: bridging tumor cells and the tumor vasculature. *Front. Oncol.* **14**, 1408051 (2024).
21. Guo, Z. et al. Tumor angiogenesis and anti-angiogenic therapy. *Chin. Med. J. (Engl)*. **137** (17), 2043–2051 (2024).
22. Zeng, Y. & Fu, B. M. Angiogenesis and Microvascular Permeability. *Cold Spring Harb Perspect. Med.* **15** (1), a041163 (2025). Published 2025 Jan 7.
23. Cornice, J. et al. NF-κB: Governing Macrophages in Cancer. *Genes (Basel)*. **15** (2), 197 (2024).
24. Ding, M. et al. B7-H3-Induced Signaling in Lung Adenocarcinoma Cell Lines with Divergent Epidermal Growth Factor Receptor Mutation Patterns. *Biomed. Res. Int.* **2020**, 8824805 (2020).
25. Zhou, Z. Z. et al. A Dual-Payload Antibody-Drug Conjugate Targeting CD276/B7-H3 Elicits Cytotoxicity and Immune Activation in Triple-Negative Breast Cancer. *Cancer Res.* **84** (22), 3848–3863 (2024).
26. Li, Q. T. et al. Alpha-Fetoprotein Regulates the Expression of Immune-Related Proteins through the NF-κB (p65) Pathway in Hepatocellular Carcinoma Cells. *J. Oncol.* **2020**, 9327512 (2020).
27. Tian, H. et al. Clinicopathologic and ultrasonographic features of combined hepatocellular-cholangiocarcinoma and its correlation with microvascular invasion: a predictive role of contrast-enhanced ultrasound. *Front. Oncol.* **14**, 1474675 (2024). Published 2024 Dec 20.
28. Park, J., Lee, J. M., Kim, T. H. & Yoon, J. H. Imaging diagnosis of hepatocellular carcinoma: Future directions with special emphasis on hepatobiliary magnetic resonance imaging and contrast-enhanced ultrasound. *Clin. Mol. Hepatol.* **28** (3), 362–379 (2022).
29. Healthcare Engineering, J. O. & Retracted The Correlation between Targeted Contrast-Enhanced Ultrasound Imaging and Tumor Neovascularization of Ovarian Cancer Xenografts in Nude Mice. *J. Healthc. Eng.* **2023**, 9872503 (2023).
30. Xiong, X. et al. Ultrasound Molecular Imaging Enhances High-Intensity Focused Ultrasound Ablation on Liver Cancer With B7-H3-Targeted Microbubbles. *Cancer Med.* **13** (20), e70341 (2024).

Figures

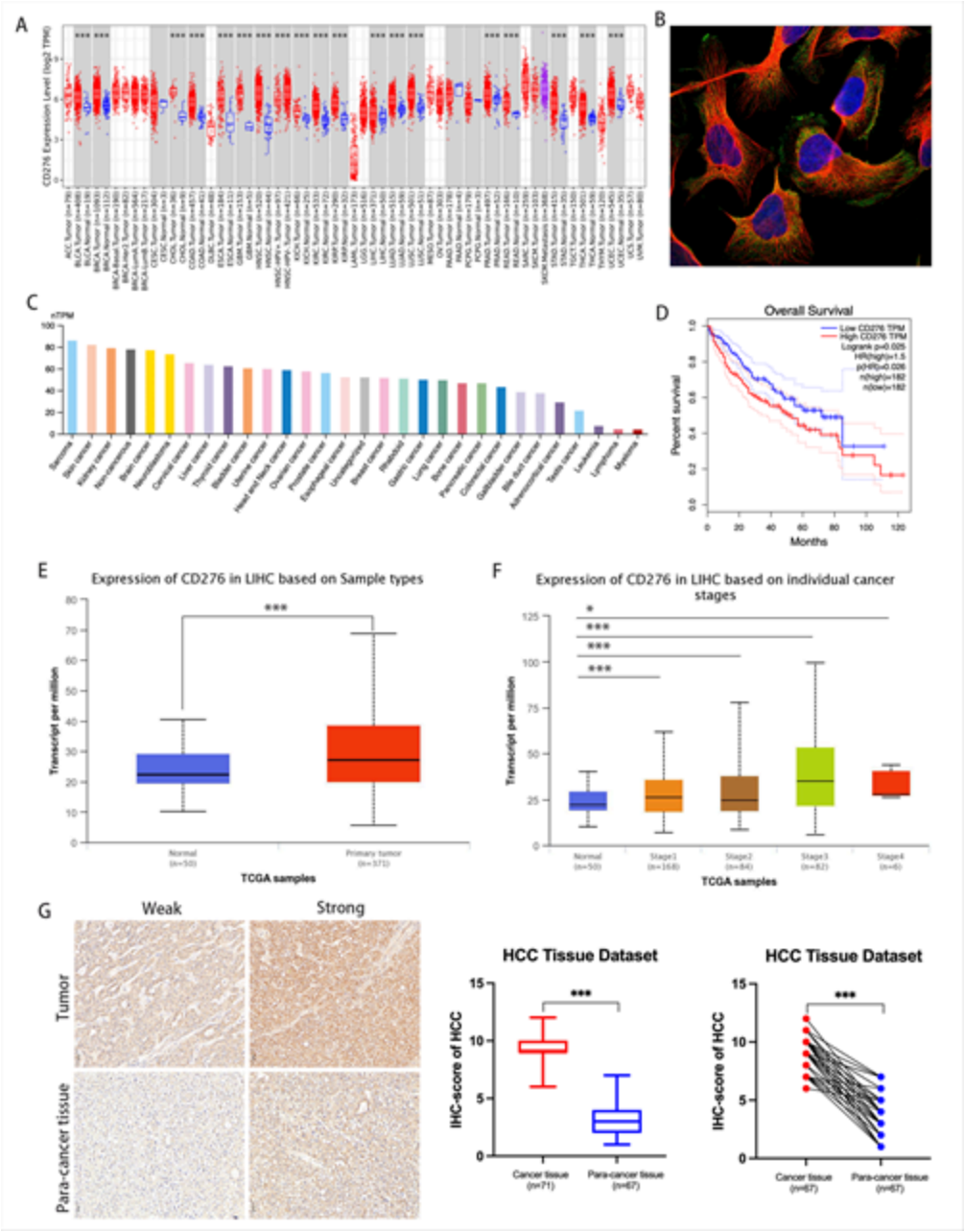


Figure 1

B7-H3 expression in HCC samples. (**A**) The expression of B7-H3 in 33 types of cancer tissues and adjacent normal tissues. (**B**) Visualization of the subcellular localization of B7-H3 (from the Human Protein Atlas database, http://www.proteinatlas.org/). The red and green fluorescence represent microtubules and B7-H3 protein respectively. (**C**) The protein expression of B7-H3 in various cancer tissues from the HPA. (**D**) The relationship between the expression of B7-H3 in the TCGA database and the survival period of patients with liver cancer. (**E, F**) Analysis based on the UALCAN online database showed that, compared with normal liver tissues, the protein expression of B7-H3 was significantly higher in liver cancer tissues. Moreover, the high expression of B7-H3 was associated with more severe clinical stages of patients. (**G**) The expression of B7-H3 in HCC tissues and their adjacent tissues was

detected by immunohistochemistry. Immunohistochemical analysis showed that the expression of B7-H3 was significantly higher in HCC tissues than that in adjacent tissues. *$p < 0.05$, ***$p < 0.001$.

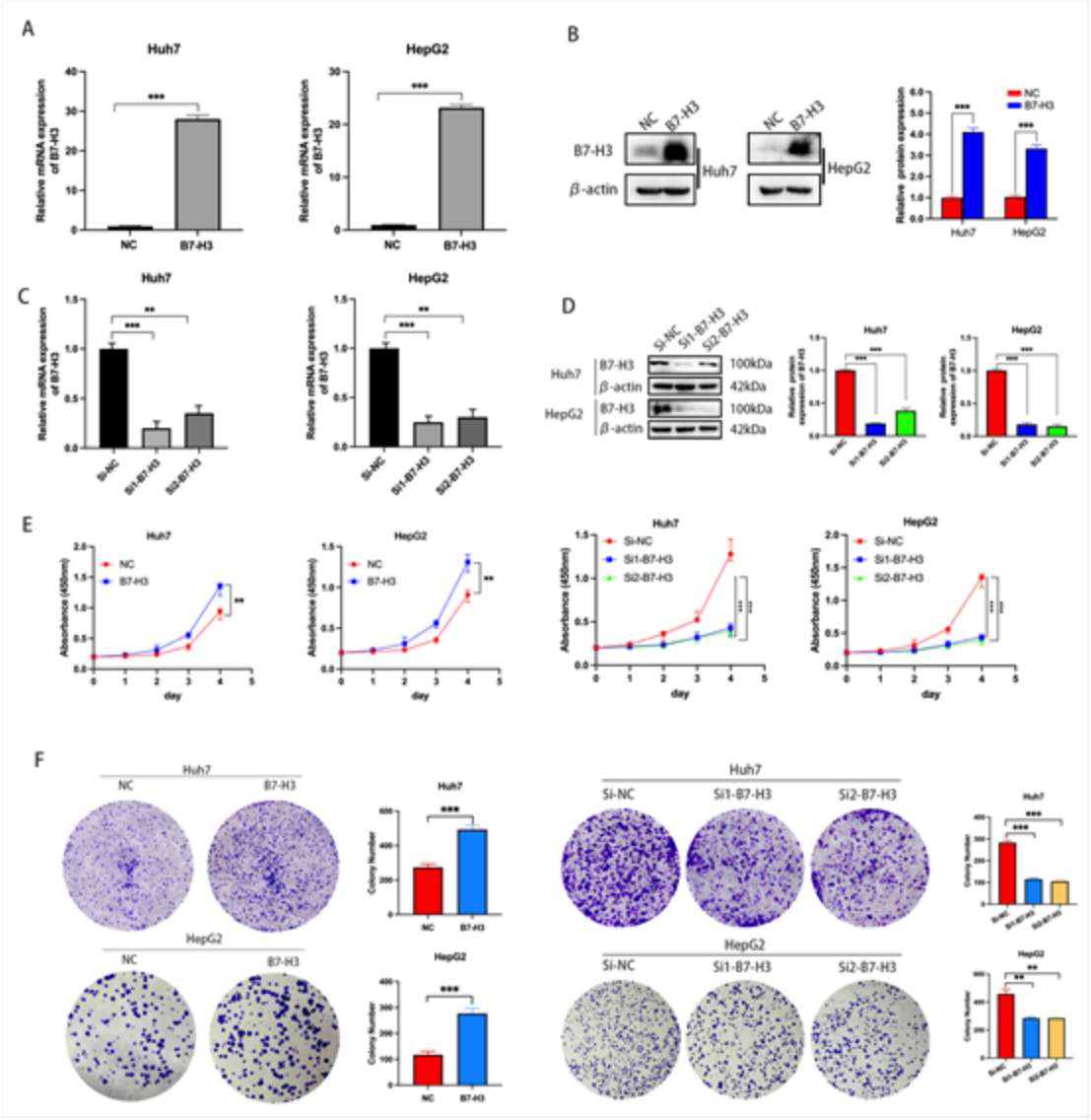


Figure 2

Construct a model of B7-H3 overexpression and silencing cell lines in HCC cells. (**A)** Verification of the overexpression efficiency of B7-H3 in Huh7 and HepG2 hepatocellular carcinoma cells by qPCR.**(B)** Verification of the overexpression efficiency of B7-H3 in Huh7 and HepG2 hepatocellular carcinoma cells by Western Blot. (**C)**Verification of the knockdown efficiency of B7-H3 in Huh7 and HepG2 hepatocellular carcinoma cells by qPCR. (**D)** Verification of the knockdown efficiency of B7-H3 in Huh7 and HepG2 hepatocellular carcinoma cells by Western Blot. (**E)** The CCK8 assay confirmed that when B7-H3 was overexpressed, the viability of HCC cells was significantly higher than that of the control group, knockdown of B7-H3 significantly inhibited the viability of Huh7 and HepG2 cells. (**F)** The plate clone formation assay showed that the clonogenic ability of HCC cells was significantly enhanced after B7-H3 overexpression compared with that of the negative control group, clonogenic ability of hepatocellular carcinoma cells was significantly reduced after B7-H3 knockdown compared with that of the negative control group. **$p < 0.01$, ***$p < 0.001$.

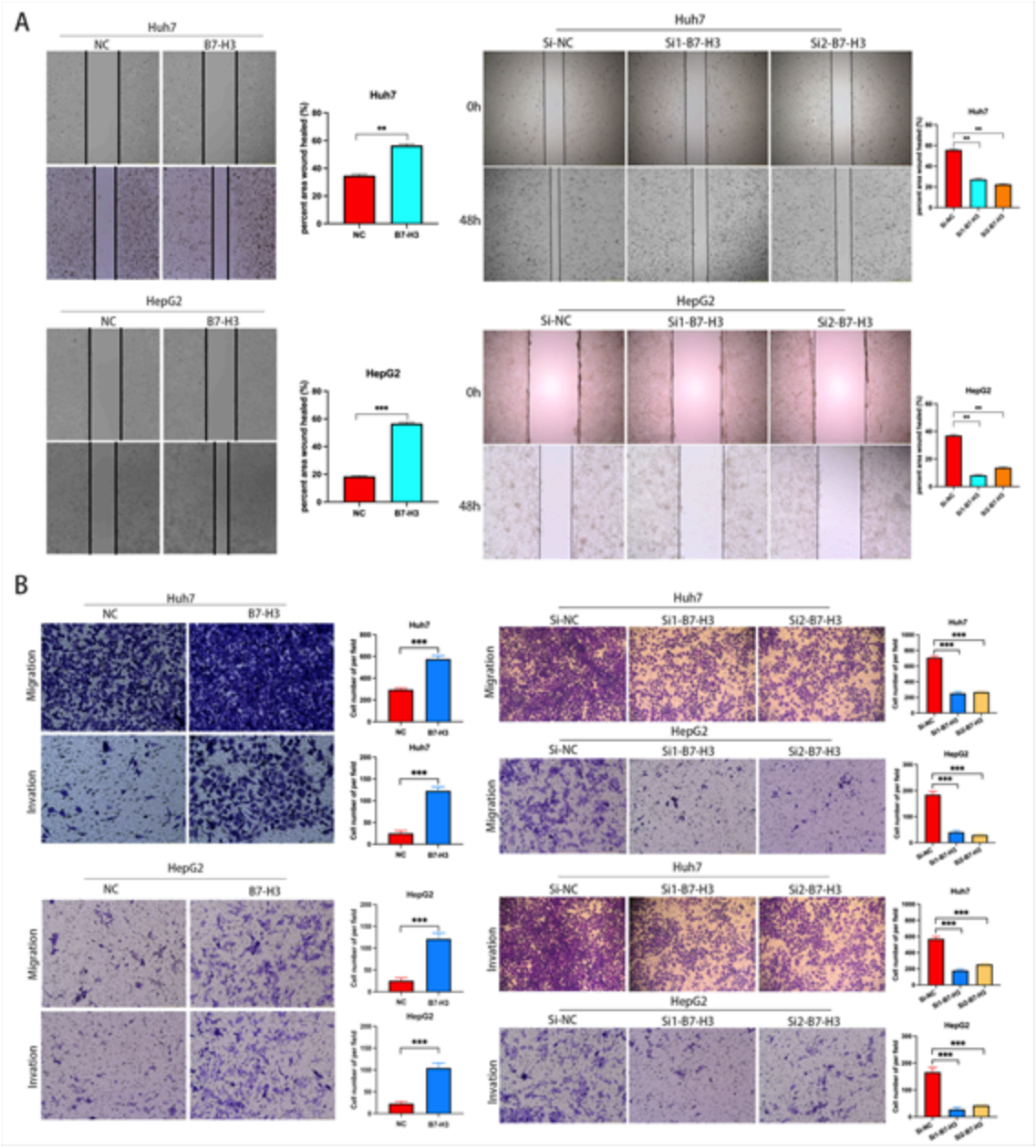


Figure 3

B7-H3 promotes HCC cell migration and invasion. (**A)** The experimental results demonstrated that B7-H3 overexpression significantly enhanced the migratory ability, and knockdown of B7-H3 significantly inhibited the migration ability of Huh7 and HepG2 cells. (**B)** The Transwell assay verified that the overexpression of B7-H3 significantly enhanced the migration and invasion abilities, and knockdown of B7-H3 significantly inhibited the migration and invasion abilities of Huh7 and HepG2 cells. $^{**}p < 0.01$, $^{***}p < 0.001$.

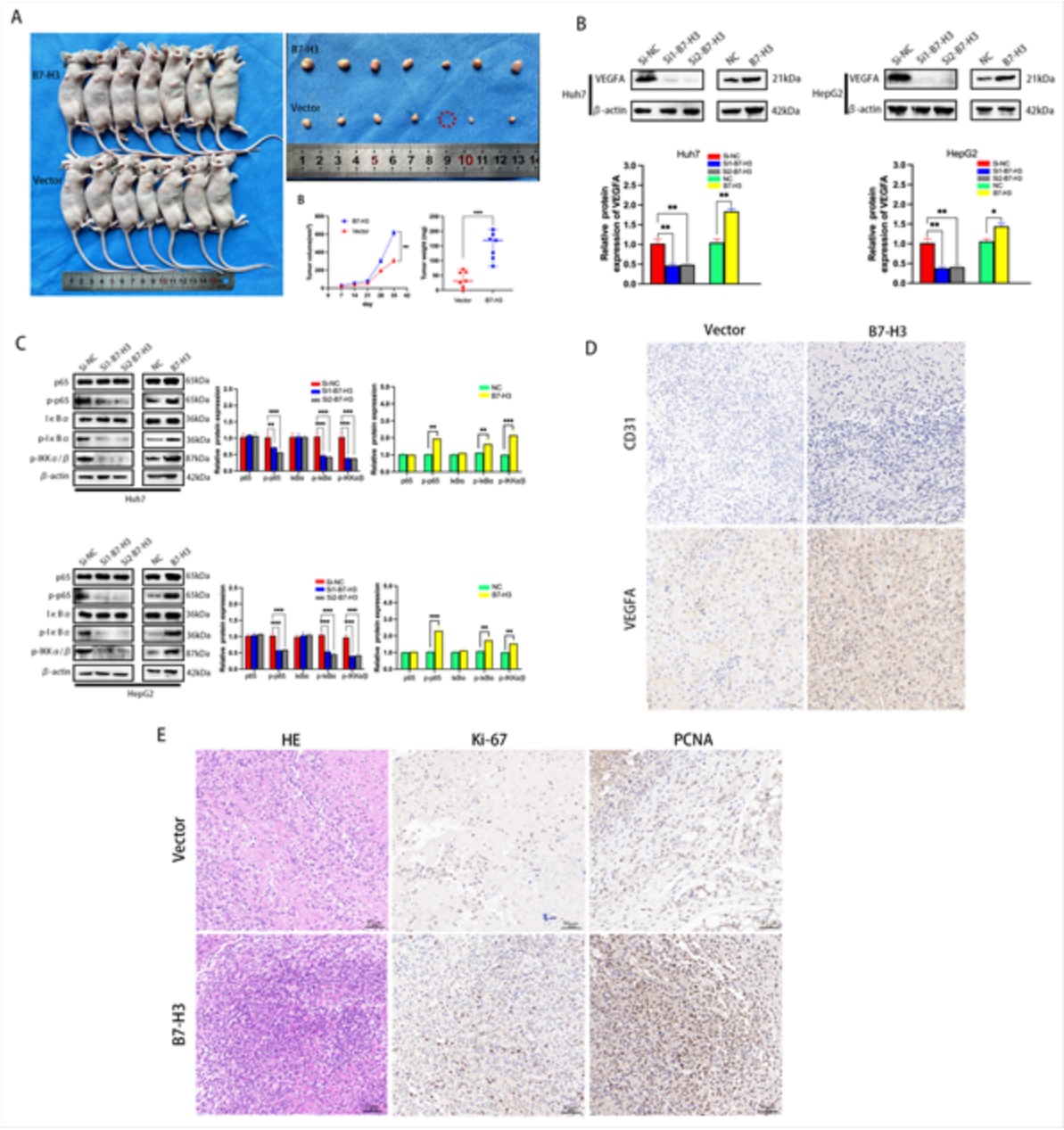


Figure 4

Establishment of tumor transplantation models in nude mice. (**A)** The nude mice were sacrificed 35 days after the injection of tumor cells, and the subcutaneous tumors were taken out for observation. The tumor size (width²×length×π/6) was measured with a vernier caliper every 7 days. The growth curve of the xenograft tumors was plotted, and the xenograft tumors were removed and weighed. (**B)** Western Blot was used to analyze the regulation of VEGFA by the overexpression or silencing of B7-H3 in Huh7 and HepG2 cells. (**C)** The protein expression of the NF-κB signaling pathway in Huh7 and HepG2 cells was detected by Western Blot. (**D)** Immunohistochemistry (IHC) for the expression of VEGFA and CD31 in the subcutaneous xenograft tumors of nude mice. (**E)** Immunohistochemistry (IHC) for the expression of HE, PCNA and Ki-67 in the subcutaneous xenograft tumors of nude mice. *$p < 0.05$, **$p < 0.01$, ***$p < 0.001$.

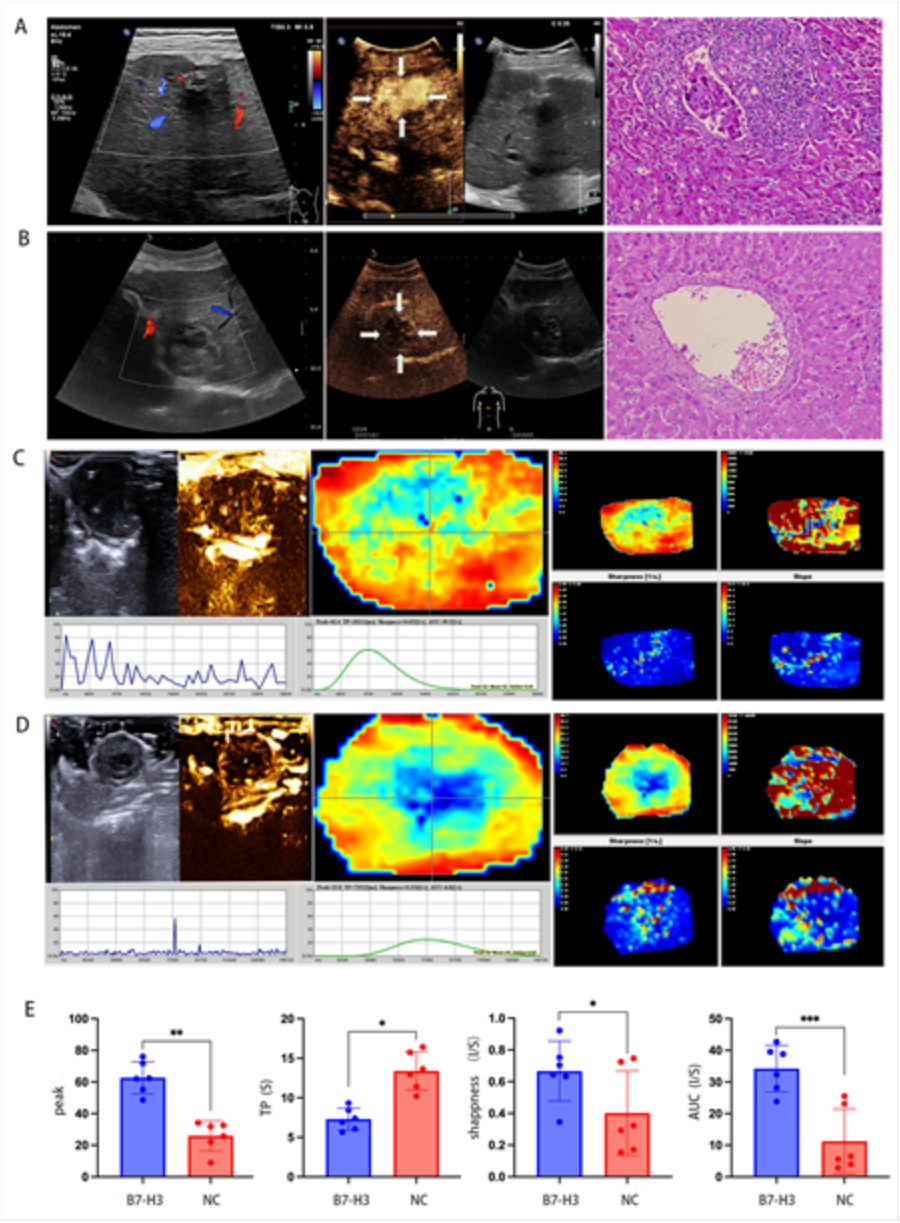


Figure 5

The correlation between B7-H3 expression and contrast-enhanced ultrasound manifestations. (**A)** Male, 56 years old, pathologically confirmed HCC with microvascular invasion. B7-H3 exhibited high expression, and CEUS demonstrated hyperenhancement during the arterial phase. (**B)** Male, 67 years old, pathologically confirmed HCC without microvascular invasion. B7-H3 showed low expression, and CEUS revealed hypoenhancement during the arterial phase. (**C)** The contrast-enhanced ultrasound curve of the xenograft tumors in the B7-H3 overexpression group. (**D)** The contrast-enhanced ultrasound curve of the xenograft tumors in the control group. (**E)** The contrast-enhanced ultrasound parameters of the xenograft tumors in the two groups, including peak value, time to peak (TP), sharpness (perfusion rate), and area under the curve (AUC, perfusion volume), all showed statistical significance. *$p < 0.05$, **$p < 0.01$, ***$p < 0.001$.